Sizing the Stack: Predicting Stack Heights Using Satellite Imagery

Dean Huang, Nikhil Bhargava, Xiaohan Yang, Yijia Zhang

Duke MIDS Capstone Report

ABSTRACT

The goal of this project was to estimate the heights of power plant stacks from publicly available satellite imagery data. Our client, *WattTime*, is working to build the first automated system to monitor emissions from power plants globally, utilizing the height of flue-gas stacks to better understand the dispersal of pollutants as well as the contribution of power plants to climate change. Our team created an automated pipeline to download satellite imagery, process images, estimate the length of shadows cast by plant stacks, and used physics-based approaches to predicting stack heights. Ultimately, we used this tool to generate the first comprehensive database of power plant stack heights for over 16,000 power plant stacks worldwide.

1. INTRODUCTION

Burning fossil fuels is one of the major sources of greenhouse gas (GHG) emissions into the atmosphere and causes of global climate change [1]. In particular, fossil fuel-based power plants account for 30% of annual GHG emissions. This equates to nearly 15 billion tons of CO2 released into the atmosphere every year. These plants, however, are critical for power production and account for roughly 67% of all global electricity generation worldwide [2]. The energy generated by these power plants is primarily produced by combusting fossil fuels such as coal, natural gas, and oil, which result in the production of GHG as well as other air pollutants such as sulfur dioxide (SO2), carbon dioxide (CO2), and nitrogen oxides (NO).

In order to monitor and mitigate the effects of climate change, it's critical to better understand the source and amount of emissions generated at a power plant level [1]. The ability to monitor the dispersion of these air pollutants is key to studying how power plants impact the local community, the broader environment, and climate change. Additionally, tracking the dispersion of pollutants is crucial for policymakers, scientists, and companies to design and implement viable and effective sustainability strategies. Although a few countries, such as the United States, have systems to monitor emissions and publicly report this information, it's infeasible and impractical for many countries to monitor and report such emissions.

Currently, coalitions such as *Climate TRACE* are working with partners to enable emissions tracking through the use of satellite imagery, remote sensing, and artificial intelligence [3]. Our client, *WattTime*, a Climate TRACE member, aims to build the first automated system to monitor emission production and transportation for every power plant in the world. Using information such as the operational status of a power plant, weather data, and plant flue-stack heights, *WattTime* aims to estimate and monitor the total amount and dispersion of pollutants produced by every power generating station in the world. One key missing input to this equation is the flue-gas stack heights across power plants globally.

This paper is centered around our approach to predicting global flue-gas stack heights using satellite imagery and associated metadata. Additionally, we discuss the use of these methods to create the world's first database of power plant stack heights across the

globe, containing over 16,000 estimates of power plant stack heights. This information will enable *WattTime* to begin the process of monitoring global power plant emissions at a more granular level.

2. BACKGROUND

Concentrations of CO2 are currently measured globally by two satellite missions: the Orbiting Carbon Observatory (OCO-2) and the Greenhouse Gases Observing Satellite (GOSAT) [1]. These two satellites utilize spectroscopic methods based on the absorption of reflected sunlight to estimate the column-averaged dry-air mole fraction of CO2, known as XCO2. However, using XCO2 to estimate emissions from power plants is difficult and unreliable because GHG concentrations are also caused by natural sources such as CO2 and methane released from biomass decomposition.

WattTime aims to bypass this approach to monitoring GHG from power plants and other industrial facilities across the globe by estimating the height of flue-gas stacks of power plants using satellite imagery. This will allow them to better understand the dispersal of pollutants into the environment, in communities, as well as how power plants contribute to climate change. Stack heights are one of the crucial factors that contribute to the interstate transportation of air pollution. Tall stacks generally disperse pollutants over greater distances than short stacks and provide pollutants with greater time to react in the atmosphere to form ozone and particulate matter [4].

Power plant stacks come in varying shapes and sizes, ranging from tens to hundreds of meters, and there is currently no comprehensive database that contains stack heights for power plants globally. While little work has been done measuring stack heights using satellite imagery, others have done similar tasks using shadows of objects such as trees and physics-based methods to recreate the height of vegetation patches using tree shadows [5]. Other, more advanced methods, have also been used to recreate the height of buildings with the use of expensive tools such as LiDAR or computer vision models trained on large quantities of privately labeled data [6, 7]. Additionally, while extensive research has been done in detecting shadows pixels in high spatial resolution aerial imagery, height prediction techniques have not been applied to satellite imagery due to a lack of solar position metadata not tracked with aerial imagery [8]. Aerial imagery is also expensive to acquire and thus more difficult to use on a global scale.

Ultimately, we approach the problem by making use of physics-based approaches regarding the shadows of objects, more specifically plant stacks, with regards to the

geospatial location of satellites. Based on the time of day a satellite image was taken, the position of the sun with regards to the satellite, and the length of a shadow, one can successfully make an estimate of how tall an object is. A visual representation for estimating the height of a stack using this process is shown in Figure 1 below. While the timestamp of a satellite image and the position of the sun at the time an image was taken are recorded by satellites, the shadow length of a stack is the missing piece of the equation to estimating the height of a stack

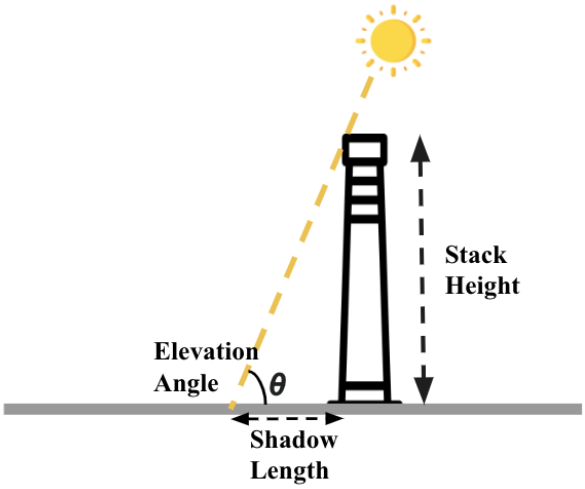

Physics Based Model

Stack Height = tan(θ) × Shadow Length

- Solar Elevation Angle (θ)
  (Sentinel-2 Metadata)
- Shadow Length
  (Automated Pipeline)

Figure 1: Physics-based approach to estimating stack heights.

3. DATA

To acquire satellite images of stack shadows, we utilized geographic coordinates (latitude and longitude) of targeted stack bases, provided by *WattTime*. They have made significant contributions to the geographic database of Open Street Maps (OSM) by providing manual annotations of power plant stack bases on a global scale. Using the annotated stack base coordinates, we downloaded four Sentinel-2 spectral bands with a spatial pixel resolution of 10 meters. Sentinel-2 satellite imagery was used as they are publicly available, have global image coverage, and have relatively high image resolution. Of the four bands, or channels, provided, three are natural color bands (red, green, and blue channels) that make up the visible spectrum our eyes see, and the fourth is a near-infrared band [9]. The purpose of the near-infrared band is to help identify surrounding vegetation and was used primarily in the Shadow Detector Index shadow length estimation method described further in *Appendix B*.

Additionally, to estimate the height of each stack, metadata associated with each

Sentinel-2 image, such as the Mean Solar Azimuth angle, the Mean Solar Zenith angle, and the Timestamp of each image was acquired. More information regarding the use and descriptions of these features can be found in *Appendix A*. Lastly, ground truth information on stack heights from the US Energy Information Administration (EIA), which provides annual data on the status of existing electric generating plants and associated equipment in the United States and Puerto Rico, were used to validate stack height estimation methods described in further sections.

4. METHODS

To predict the height of plant stacks, we developed an automated pipeline that ingests Sentinel-2 satellite images, along with associated metadata, and outputs predicted stack heights. Our pipeline can be broken down into four stages: Satellite Imagery Download, Image Processing, Shadow Length Calculation, and Stack Height Prediction (Figure 2). Each stage will be described in greater detail in the sections below. While many shadow length estimation techniques were tested to minimize validation error, this paper will only cover the optimal approach used to create the final global stack height database. Refer to *Appendix B* to learn more about the other approaches tested and their respective validation accuracy.

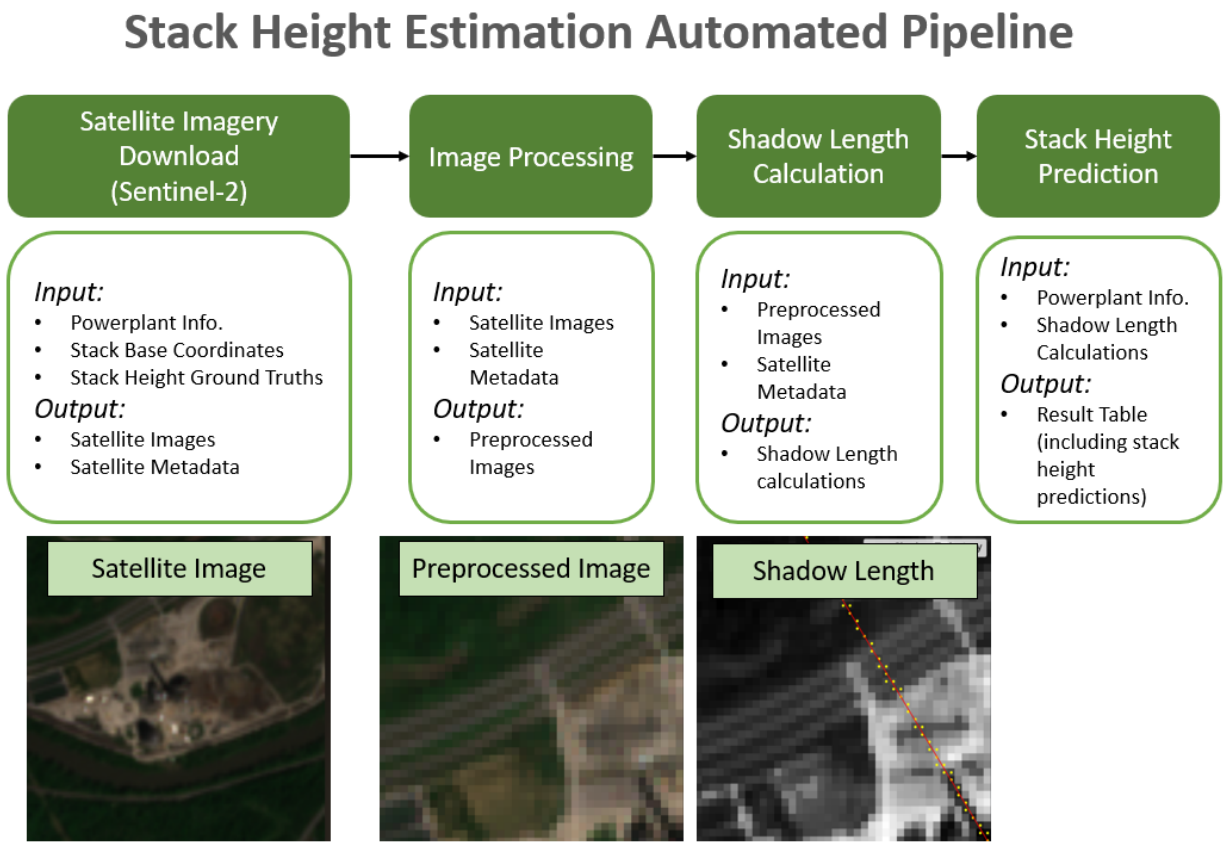

Figure 2: Automated stack height estimation pipeline.

4.1 SATELLITE IMAGERY DOWNLOAD

Using geographic coordinates of stack base locations annotated by *WattTime*, Sentinel-2 imagery of stack bases was downloaded utilizing the Google Earth Engine API. Each image downloaded contained a physical surface area of 1000m x 1000m, centered around the base of each stack, also known as the Area of Interest (AOI). This was done to ensure even the largest stack shadows would be contained within the AOI. Additionally, multiple images of each stack were downloaded during the winter months of the plant location (April 2020 to September 2020 for plants in the Southern Hemisphere and October 2020 to March 2021 in the Northern Hemisphere) as those are months in which shadows are the longest, and as a function of our physics-based model, are less prone to errors in predicting stack height. Lastly, images that had cloud coverage of greater than 5% were excluded to ensure high visibility of stack shadows. Associated image metadata, such as the Mean Solar Azimuth Angle, Mean Solar Zenith Angle, and Timestamp of each image were also downloaded. The definition of each value in the metadata and their

respective use case can be found in *Appendix A*.

4.2 IMAGE PROCESSING

Once stack satellite images were acquired, the next step was processing the downloaded images to facilitate shadow length estimation methods. The two primary components of this step were cropping each image cropping and converting them to grayscale.

Each stack image was cropped based on the expected location of the stack shadow to increase the signal-to-noise ratio by excluding irrelevant pixels. Utilizing the mean solar azimuth angle, the expected quadrant (upper left, bottom left, bottom right, and upper right) of the stack shadow was identified, and the image was cropped to contain only the relevant quadrant (Figure 2).

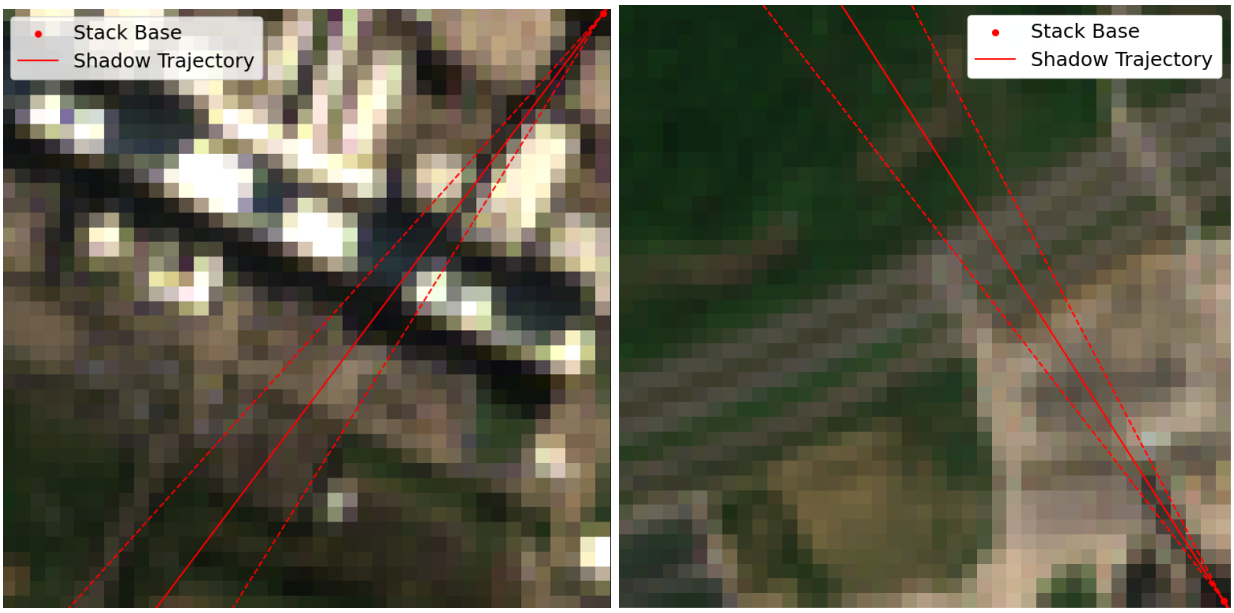

Figure 3: Examples of satellite imagery containing stack shadows located in the lower left (Left) and upper left (Right) quadrants. The red dot indicates the location of the stack base, the solid red line represents the expected shadow trajectory of a plant stack shadow calculated based on the Solar Azimuth Angle, and the dashed red lines are confidence bands of where the shadow is expected to lie.

In addition to image cropping, each image was converted from RGB to grayscale to simplify the problem. This was done by computing the weighted average along each R, G, and B value for each pixel in an image. Each pixel was then represented by an intensity value between 0 and 1 rather than 3 RGB values. Pixels with lower intensity values indicate darker pixels, while higher intensity values represent lighter pixels.

4.3 SHADOW LENGTH CALCULATION

Using the physics behind where the expected shadow of a stack is to fall, the shadow length was calculated. Equation 1 below contains the formula for calculating the slope of the expected shadow angle.

$$\theta: \textit{mean solar azimuth angle}$$

$$slope = tan((90 - |180 - \theta|) * \frac{\pi}{180}) \quad (1)$$

This slope was used to linearly identify all potential pixels on the expected shadow line of a stack as shown in Figure 3. This allowed for the problem to be simplified by reducing the need to classify all intensity values in a 2-Dimensional image to a 1-Dimensional array of pixel intensity values along the expected shadow line. Additionally, to minimize potential errors in intensity values due to noise in image quality, the minimum intensity value of neighboring pixels along the expected shadow line was chosen to represent the pixel intensity value for each pixel on the line.

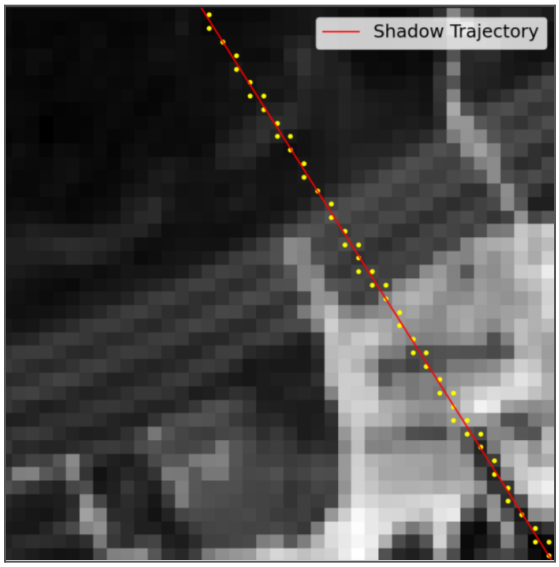

Figure 4: Potential shadow pixels on the expected shadow trajectory line. The red line indicates the expected shadow trajectory line and the yellow dots indicate potential shadow pixels intersecting the line.

Given pixels closer to the stack base are likely stack shadow pixels, we expect intensity values early in the 1-Dimensional array to be stack shadow pixels and gradually transition to non-shadow pixels. This concept is visually depicted in Figure 4 below.

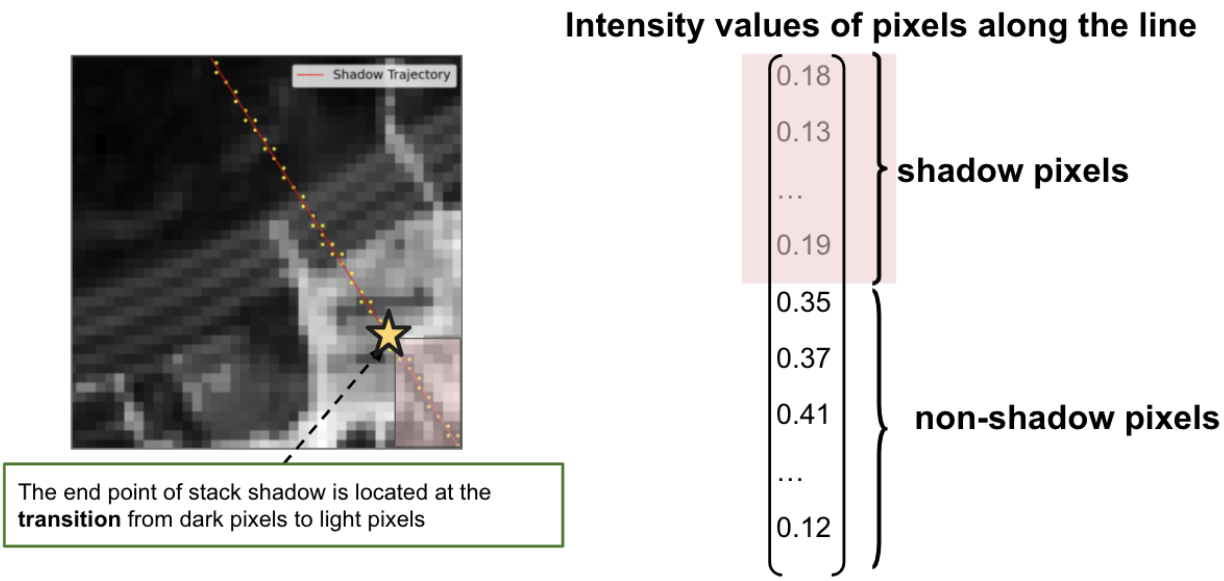

Figure 5: Visualizing the 1-Dimensional array of pixel intensity values along the expected shadow trajectory line.

In order to determine which pixels were associated with the potential stack shadow, we utilized the change point detection algorithm to classify shadow pixels. The goal of change point detection is to identify positions in a series where the mean value of those positions change. Therefore, change point detection allowed us to find significant spikes in intensity values along expected shadow lines and treat the index of specific change points as potential endpoints of the stack shadow (Figure 5).

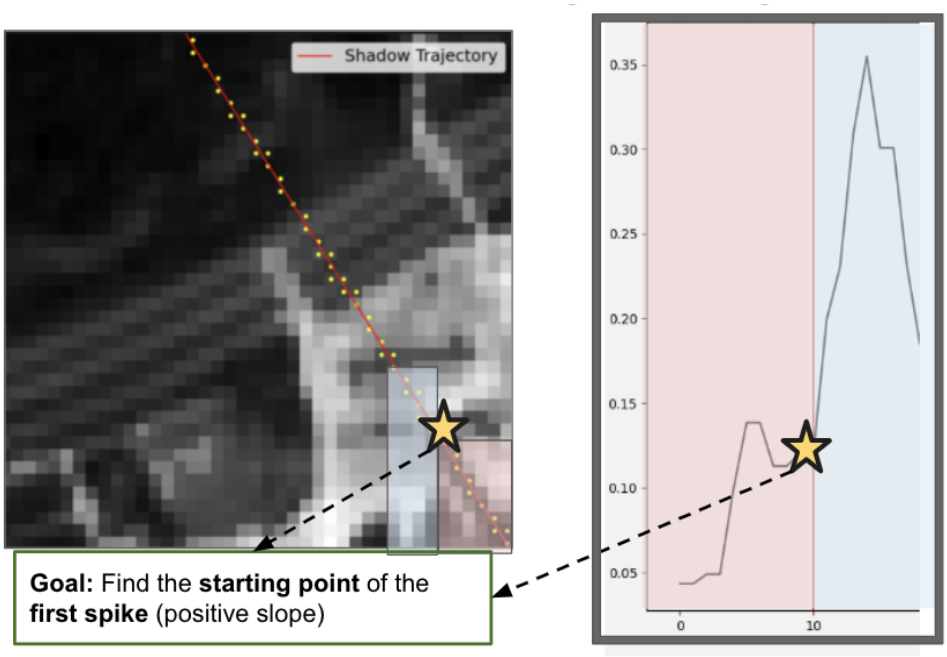

Figure 6: Identifying the end point of a stack shadow using the first transition from low intensity to high pixel intensity values.

Two key parameters, the number of change points detected and which change point indicated the end of the shadow were optimized by minimizing the validation metrics during the experimentation process discussed below. Through experimentation, we found the optimal parameters to be identifying four change points and choosing the first change point with a positive slope, indicating the first change from darker pixels to lighter pixels. Figure 5 visually depicts the process of using change point detection to determine the location of each change point in the pixel intensity array and selecting the first positive slope change to classify stack shadow pixels.

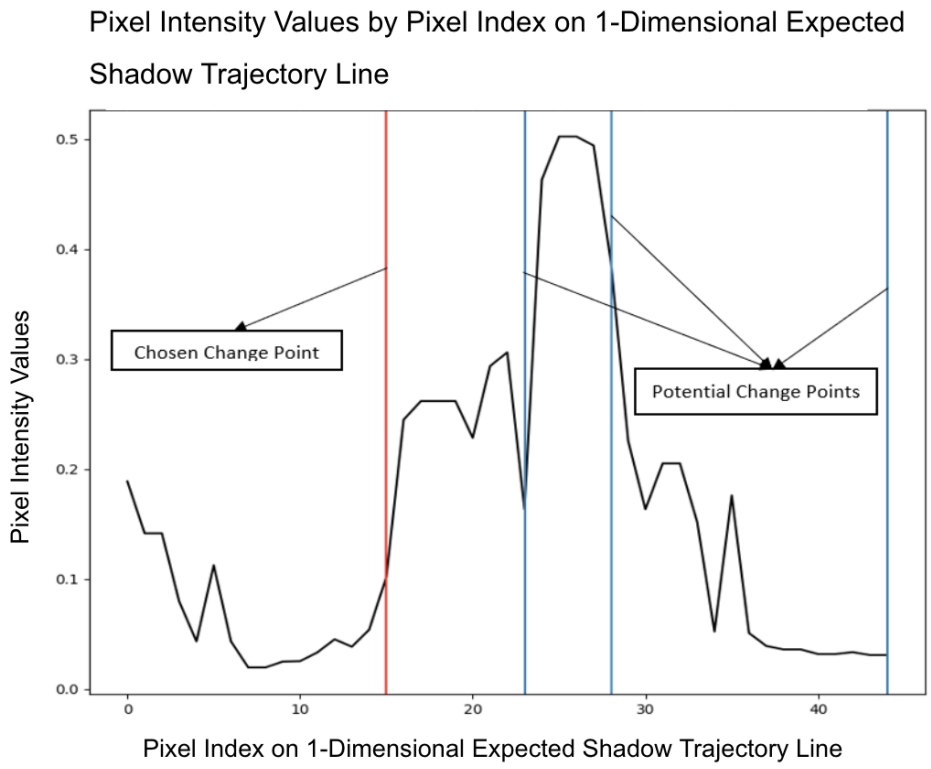

Figure 7: Pixel intensity values by pixel index on expected shadow trajectory line. The vertical lines represent all change points detected by the algorithm, while the red vertical line indicates the change point selected (first positive slope change point) as shadow cutoff.

Once all potential shadow pixels were classified, the shadow length was calculated using the Pythagorean Theorem. The distance of the furthest shadow pixel in the x and y directions from the stack base in the image corresponds with the sides of a triangle in the equation, while the hypotenuse of the created triangle is equivalent to the length of the predicted shadow.

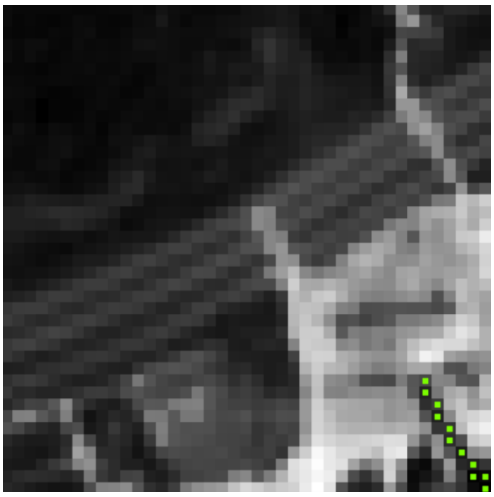

Figure 8: Grayscale satellite image of a stack shadow in the Big Bend power plant in Gibston, Florida. Green squares indicate pixels classified as stack shadow.

4.4 STACK HEIGHT PREDICTION

To estimate the height of each stack, we adopted a physics-based approach. Based on the shadow length calculated from each satellite image and the mean zenith angle (θ) of the sun (angle between the sun's rays and the vertical direction), the height of each power plant stack can be calculated. This formula can be found below and is visually represented in Figure 1 above.

$$Stack\ Height\ =\ tan(90\ -\ \theta)\ *\ Shadow\ Length \quad (2)$$

Since each stack had roughly 10 to 58 images taken over time (the number of images returned was dependent on the filtering criteria discussed in section 4.1), it was necessary to determine one optimal prediction per stack. In order to make this prediction, the pipeline made a prediction for each image of a stack. The median of these predictions for each power plant stack was then used as the final prediction for the height of the stack. Due to the likelihood of the prediction distribution of stack heights being skewed with outliers, this process was akin to removing poor predictions potentially caused by poor image quality or shadow length estimation error in an automated fashion. Ultimately, we found this approach to have greater validation accuracy than making a single prediction on one image of a stack.

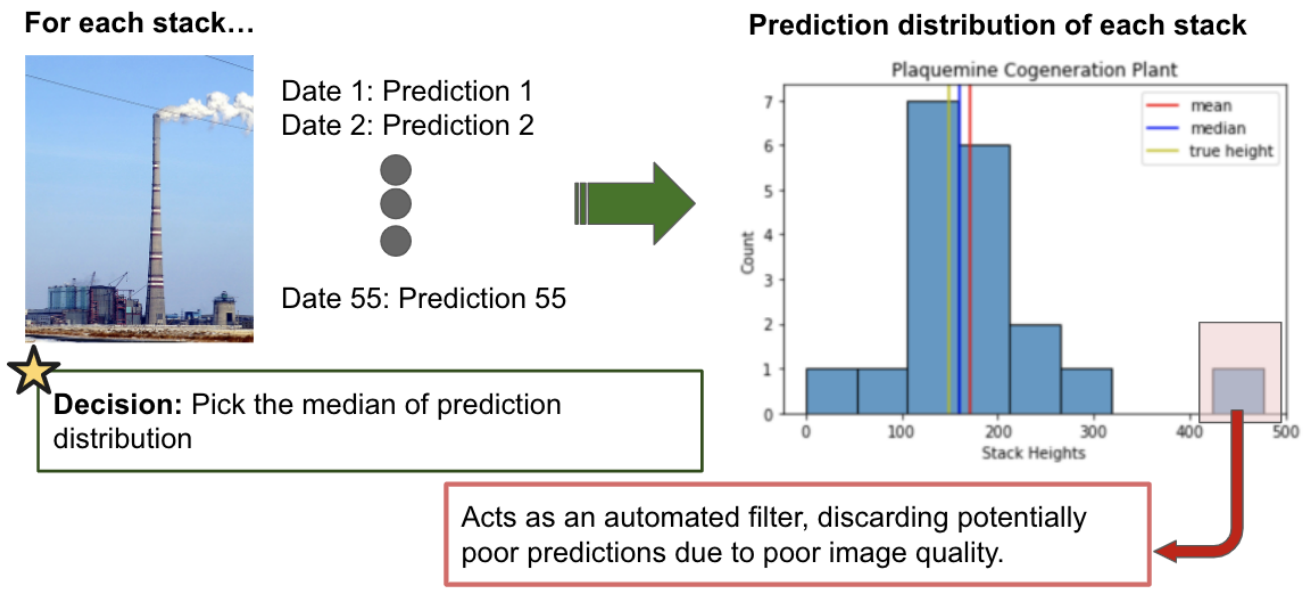

Figure 9: Distribution of predicted stack heights for the Plaquemine power plant in Plaquemine, Louisiana. The median stack height (indicated in blue) was chosen as the stack height prediction for the plant. The true height of the plant is indicated by the yellow line.

5. EXPERIMENT SETUP & RESULTS

To evaluate the results of each of our shadow length estimation methods, and as a result our stack height predictions, we curated a diverse dataset of 94 power plant stacks across the US, with ground truth data extracted from the EIA database. This dataset included power plants from over 40 states across the US, relatively small and large power plants, as well as different types of plants such as coal and gas-fired power plants. Since a physics-based approach was used for stack height prediction, there was no need for a traditional train and test split, and this dataset was used as a validation set.

To evaluate our predictions, we looked at three evaluation metrics: Mean Absolute Error (MAE), Mean Absolute Percentage Error (MAPE), and Root Mean Square Error (RMSE). RMSE represents how well our model performs through the calculation of residuals, while MAPE and MAE represent the absolute error and percentage error we expect when applying our model to unseen stacks.

$$MAE = \frac{1}{n}\sum_{i=1}^{n} |ground\ truth - predicted|$$

$$MAPE = \frac{1}{n}\sum_{i=1}^{n}\frac{|ground\ truth - predicted|}{ground\ truth}$$

$$RMSE = \sqrt{\sum_{i=1}^{n}\frac{(predicted - ground\ truth)^2}{n}}$$

The results of each of the methods described above can be found in Table 1 below. Additionally, we compared our methods against a naive baseline of using the median stack height in the EIA database as a prediction for every stack height.

Table 1: Accuracy of Each Stack Height Prediction Method (MAE, MAPE, RMSE)

Approach	Mean Absolute Error (ft)	Mean Percentage Error (%)	RMSE
Naive Baseline (Median)	177.66	44.04	242.11
Connected Components	300.75	125.67	412.34
RGB Shadow Detector Index	169.19	63.4	242.34
Change Point Detection	**138.01**	**32.87**	**158.95**

Ultimately, the change point detection method was selected for predicting stack heights as it minimized all three key metrics observed. It outperformed the naive baseline of predicting the median stack height in the EIA database for every power plant, as well as all other methods tested. We also believe that as this approach was scaled abroad, the change point detection method would outperform the naive baseline as the median stack height in the EIA database, or in the United States, is not representative of stacks around the world.

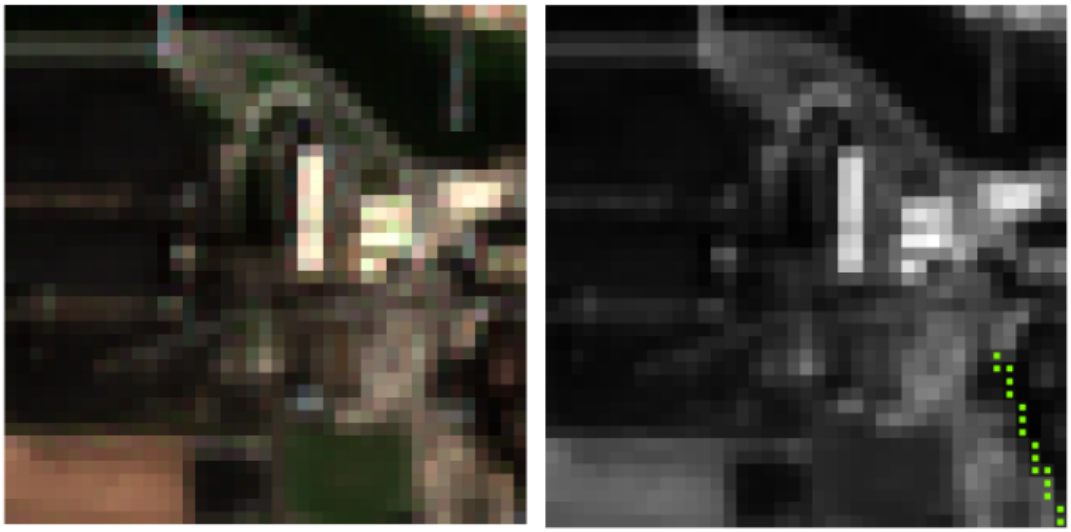

Figure 10: Example of good stack height predictions using change point detection

6. SCALING UP: CREATING A GLOBAL DATABASE OF STACK HEIGHTS

The ultimate goal of this project was to create a comprehensive dataset on power plant stack heights across the world. Using power plant stack base coordinates annotated by *WattTime*, we applied our automated pipeline to generate the first database of global stack heights containing 16,258 unique stack height predictions from 3,165 power plants. This collection of stack heights included plants from six different continents in over 50 different countries and is visualized geographically in Figure 11 below.

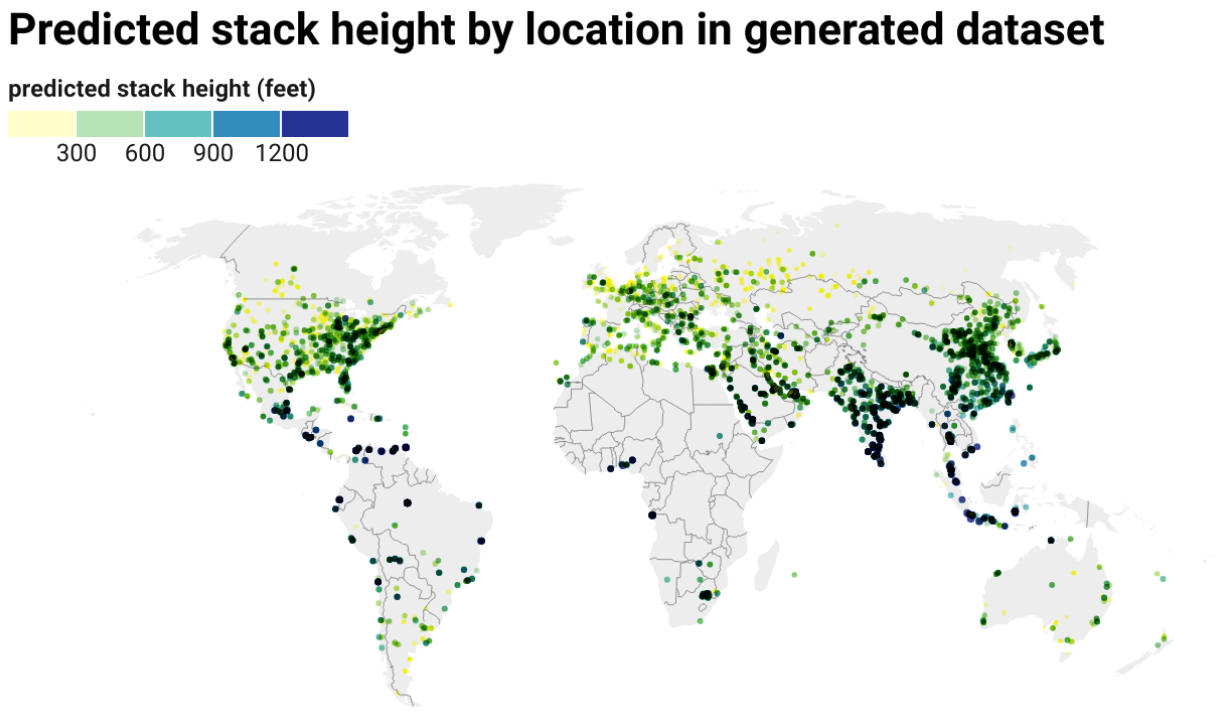

Figure 11: Predicted stack height by location in our generated database (color represents predicted heights).

From Figure 11, we discovered some of the tallest predicted stacks were found to be from power plants located in the United States, India, and China. Although there's no means of verifying the actual height of those stacks, these findings matched our expectations as some of the largest fossil-fuel-based power plants are located in those regions [10].

The distribution of predicted plant stack heights in the generated database can be found in Figure 12 below. The average plant stack height was found to be roughly 348 ft, while the median stack height was 280 ft. This was slightly larger than the median stack height of 200 ft for power plants in the US contained in the EIA database.

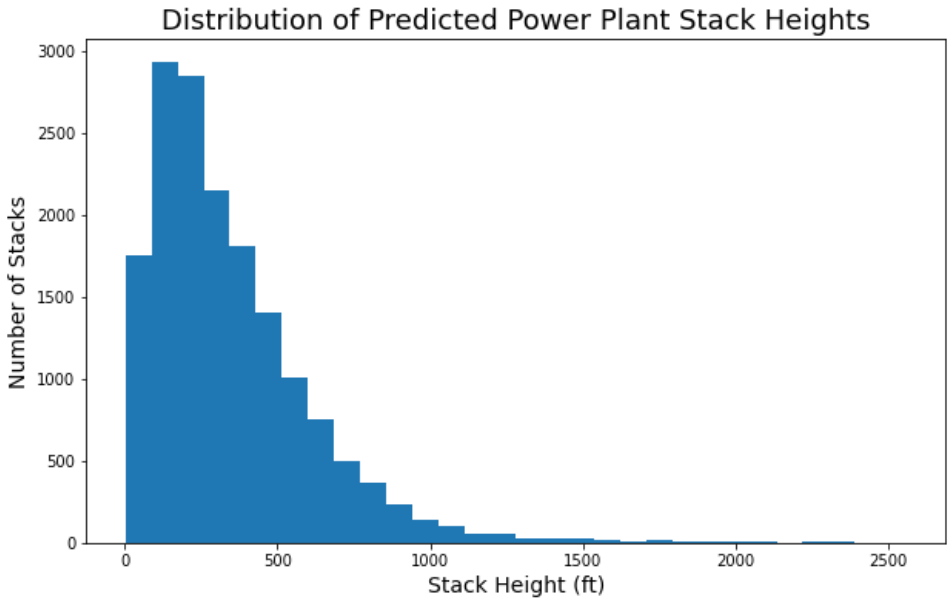

Figure 12: Distribution of predicted plant stack heights from the generated database.

7. CONCLUSION & FUTURE WORK

The purpose of this project was to create a tool to accurately predict the height of a stack given its geolocation and ultimately create the world's first database of global stack heights. Through our research, we proved the task could be done with relative confidence using Sentinel-2 satellite imagery. Ultimately, we found that the change point detection algorithm described above was the most accurate way of determining the height of a stack out of the various methods tested. The generated database of global power plant stack heights will assist *WattTime* in its goal of monitoring the dispersion of pollutants and the amount of emissions produced at a power plant level. As *WattTime* continues to annotate power plant stack base locations on OSM, this tool can be used to predict the height of new stacks added to the database.

Although significant progress has been made towards creating a comprehensive database of power plant stack heights, additional future work could be done to improve the accuracy of predictions. Another physics-based approach that could be tested, would be to include a temporal component to stack height estimation, given that our pipeline downloads satellite images of stacks over time. While stack shadow lengths vary by month, the stack height prediction should remain constant. Using both the understanding of the sinusoidal pattern of annual shadow length changes over the course of the year and constant stack height predictions, this approach may enable for

more accurate stack height predictions. Additionally, other non-physics-based approaches could be tested to estimate stack shadow length. Computer vision approaches such as object detection could potentially identify stack shadow pixels. However, this would require a larger initiative of labeling shadows in a large corpus of satellite imagery.

Another potentially effective approach to improving current stack height estimation techniques would be to replace Sentinel-2 imagery with higher resolution satellite imagery. While one shortcoming of the current change point detection method is identifying distractions in stack shadows as potential change points, higher resolution imagery that more accurately depicts the Earth's surface being captured could potentially solve this issue. Private companies such as *Planet* provide global high-resolution satellite imagery at resolutions of up to 3 meters per pixel, roughly three times higher than Sentinel-2 satellites. This, however, could make data acquisition more costly and difficult as Sentinel-2 data is publicly available.

REFERENCES

1. Couture, Heather, et al. "Towards tracking the emissions of every power plant on the planet." NeurIPS Workshop. Vol. 3. 2020.
2. Nierop and Simon Humperdinck. “International comparison of fossil power efficiency and CO2 intensity – Update 2018.” ECOFYS (2018)
3. Climate TRACE. “ABOUT CLIMATE TRACE”. Climate TRACE (2022), https://www.climatetrace.org/about
4. Trimble, David C. AIR QUALITY: information on tall smokestacks and their contribution to interstate transport of air pollution. DIANE Publishing, 2011.
5. Shettigara, V. K., and G. M. Sumerling. "Height determination of extended objects using shadows in SPOT images." Photogrammetric Engineering and Remote Sensing 64.1 (1998): 35-43.
6. Tolt, Gustav, Michal Shimoni, and Jörgen Ahlberg. "A shadow detection method for remote sensing images using VHR hyperspectral and LIDAR data." 2011 IEEE international geoscience and remote sensing symposium. IEEE, 2011.
7. Mou, Lichao, and Xiao Xiang Zhu. "IM2HEIGHT: Height estimation from single monocular imagery via fully residual convolutional-deconvolutional network." arXiv preprint arXiv:1802.10249 (2018).
8. Comber, Alexis, et al. "Using shadows in high-resolution imagery to determine building height." Remote sensing letters 3.7 (2012): 551-556.
9. GISGeography. “Sentinel 2 Bands and Combinations.” GIS Geography, 29 Oct. 2021, gisgeography.com/sentinel-2-bands-combinations.
10. Carbon Brief. “Mapped: The world’s coal power plants” (2019). https://www.carbonbrief.org/mapped-worlds-coal-power-plants
11. R. Meyer, M. Schlecht, and K. Chhatbar. “Solar resources for concentrating solar power (CSP) systems.” Science Direct (2012)
12. Choi, Heejeong, et al. "Real-time significant wave height estimation from raw ocean images based on 2D and 3D deep neural networks." Ocean Engineering 201 (2020): 107129.
13. Mostafa, Yasser, and Ahmed Abdelhafiz. "Accurate shadow detection from high-resolution satellite images." IEEE Geoscience and Remote Sensing Letters 14.4 (2017): 494-498.
14. Qi, Feng, John Z. Zhai, and Gaihong Dang. "Building height estimation using Google Earth." Energy and Buildings 118 (2016): 123-132.
15. Adeline, Karine RM, et al. "Shadow detection in very high spatial resolution aerial

images: A comparative study." ISPRS Journal of Photogrammetry and Remote Sensing 80 (2013): 21-38.
16. Liasis, Gregoris, and Stavros Stavrou. "Satellite images analysis for shadow detection and building height estimation." ISPRS Journal of Photogrammetry and Remote Sensing 119 (2016): 437-450.
17. Shao, Yang, Gregory N. Taff, and Stephen J. Walsh. "Shadow detection and building-height estimation using IKONOS data." International journal of remote sensing 32.22 (2011): 6929-6944.
18. Amirkolaee, Hamed Amini, and Hossein Arefi. "Height estimation from single aerial images using a deep convolutional encoder-decoder network." ISPRS journal of photogrammetry and remote sensing 149 (2019): 50-66.

APPENDIX A: METADATA DESCRIPTIONS

Table 2: Metadata Description Table

Column Name	Description
Mean Solar Azimuth Angle	The solar azimuth angle is the angle of the sun's rays measured in the horizontal plane from true south for the northern hemisphere or due north for the southern hemisphere [11]. This value was used to calculate the expected Shadow Trajectory Angle and expected Shadow Trajectory Line and obtained as metadata for an image from the Google Earth Engine API.
Mean Solar Zenith Angle	The solar azimuth angle is the angular displacement from south of the projection of beam radiation on the horizontal plane [11]. This value was used in the physics-based approach to predicting stack height and obtained as metadata for an image from the Google Earth Engine API.
Timestamp	The timestamp is the time at which the Sentinel-2 satellite took the image being returned by the Google Earth Engine API. This value was obtained as metadata for an image from the Google Earth Engine API.
Cloudy Pixel Percentage	The cloudy pixel percentage is a filter for image downloading in the Google Earth Engine API. A Cloud Pixel Percentage of 5% was used when downloading images of stacks.

APPENDIX B: ADDITIONAL SHADOW LENGTH CALCULATION METHODS

CONNECTED COMPONENTS

One potential method to segregate the stack shadow region is *Connected Components, or Blob Detection*. A blob is a group of pixel values that forms a colony or a large object that is distinguishable from its background. In the context of our problem, our pipeline identifies different blobs of "connected" shadow pixels and non-shadow pixels (Figure 13), and identifies the endpoint of the stack shadow by calculating the intersection of the shadow blob (blob that contains the stack base) and expected shadow angle.

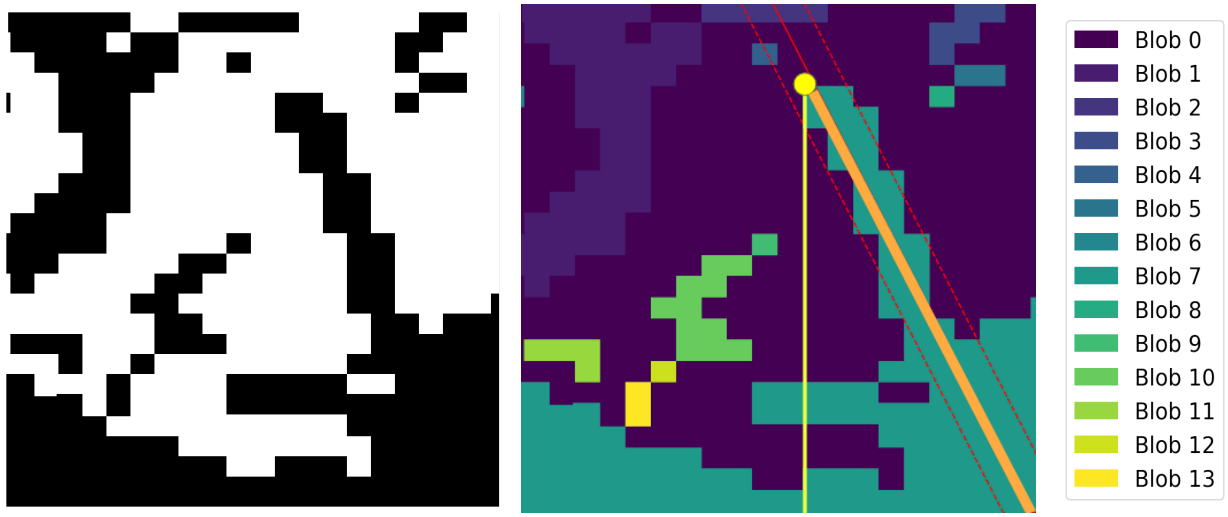

Figure 13: Original Grayscale Image (Left), Blob Detection Example (Right)

RGB SHADOW DETECTOR INDEX

The RGB Shadow Detector Index (SDI) method utilizes all four bands (Red, Green, Blue, and Near Infrared) downloaded from the Google Earth Engine API. While the rest of the pipeline remains the same, this method utilizes the use of the other bands and therefore skips the grayscaling process. Our pipeline classifies each pixel into shadow or

non-shadow pixel based on the value of the shadow detector index (SDI) [12]:

$$SDI = \frac{(1 - PC_1) + 1}{((G-B)*R)+1} \quad (1)$$

R, G, and B are normalized components of red, green, and blue bands respectively. PC_1 is a normalized component of the first principal component.

Higher value of SDI indicates a higher likelihood of the pixel being a shadow pixel. Therefore, we will specify a threshold for SDI, and classify all pixels above the threshold as shadow pixels.

Similar to *Change Point Detection*, we plot the SDI intensity graph for potential stack shadow pixels. However, we need to set a threshold for SDI to classify each potential pixel as a shadow or non-shadow pixel (Figure 6) to generate the shadow threshold graph. The threshold value we ended up setting for our pipeline was 2.1, which identified shadow pixels the best through multiple rounds of experimentations.

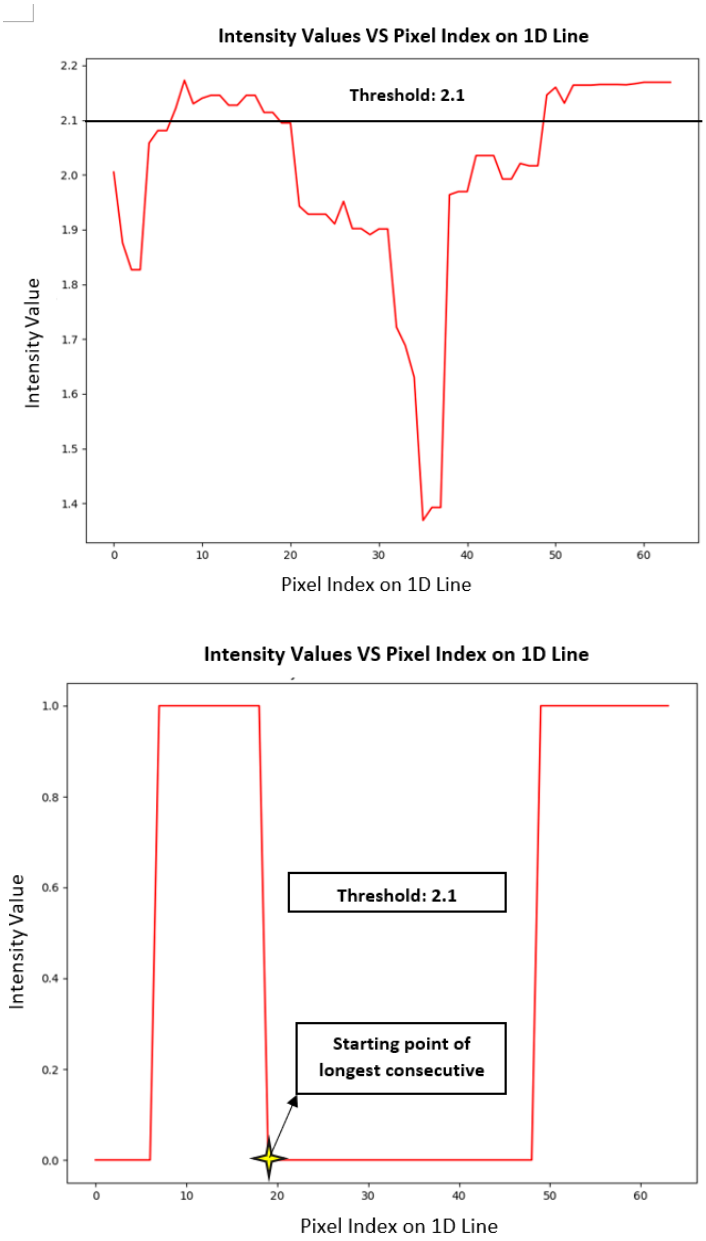

Figure 14: SDI Intensity Graph (Up), Shadow Threshold Graph (Bottom)

To find the endpoint of stack shadow, our pipeline will look at the shadow threshold graph to identify the starting point of the longest consecutive 0s (Figure 14). This starting point corresponds with where the shadow ends and a significant non-shadow region begins (Figure 14).